Appl. Phys. B 71, 495–501 (2000) / Digital Object Identifier (DOI) 10.1007/s003400000374

Applied Physics B
Lasers
and Optics

Spectral development of short pulses in KrF gain modules

T. Nagy[1], **P. Simon**[2], **S. Szatmári**[1]

[1] Department of Experimental Physics, University of Szeged, Dóm tér 9, 6720 Szeged, Hungary
(Fax: +36-62/420-154, E-mail: tnagy@physx.u-szeged.hu)
[2] Laser-Laboratorium Göttingen, Hans-Adolf-Krebs-Weg 1, 37077 Göttingen, Germany

Received: 1 November 1999/Revised version: 9 May 2000/Published online: 16 August 2000 –

Abstract. Spectral evolution of short pulses in off-axis KrF amplifiers is investigated both experimentally and theoretically. It is pointed out that the spectral features of the amplified pulses are mainly determined by the initial chirp of the pulse and the SPM in the laser windows.

PACS: 42.55G; 42.60D; 42.10

Recently, great effort has been made for the development of high-intensity UV lasers yielding $\sim 10^{19}\,\mathrm{W/cm^2}$ focused intensities at 248 nm [1–3]. The key element of such lasers is the final UV amplifier boosting up the energy of frequency-converted ultrashort seed pulses which are usually generated in the visible or near-infrared spectral range [4]. Excimers offer the possibility of efficient amplification of short UV pulses. Due to the different physical properties of excimers (smaller saturation energy and much shorter relaxation times) compared to solid-state lasers the well developed, commonly used amplification schemes – such as the CPA method – are not as efficient in excimer amplifiers as in solid-state lasers [4] (however the CPA method was successfully used in KrF amplifiers [2, 5]). For this reason an alternative technique, the so-called off-axis amplification scheme was introduced which matches the operational conditions of such amplifiers to the sharp theoretical optimum [6].

Although the gain bandwidth of excimers is significantly narrower than that of dyes or some solid-state crystals it still allows the amplification of subpicosecond pulses. This is why the spectral broadening effects – keeping the time-bandwidth product at the theoretical limit – have pronounced importance in excimer amplifiers. In this paper we investigate the different processes influencing the output pulse spectrum in KrF amplifiers. We show a way how to use these processes to reach the maximum bandwidth at the output, which is a necessary condition to reach the minimum pulse duration.

1 Experiments

The schematic view of the experimental arrangement used to study the influence of the input pulse parameters on the amplification process in a short-pulse KrF amplifier is shown in Fig. 1. Frequency-doubled 497-nm, 500-fs positively chirped pulses from a Szatmári-type dye laser system [4] were used as an input in the experiments. After frequency-doubling in a 0.3-mm-thick BBO crystal cut at 52° the pulse was directed into a pulse compressor consisting of two Brewster-angle fused silica prisms ($\varphi = 68.91°$, $n = 1.508$, $dn/d\lambda = -5.57 \times 10^{-4}\,1/\mathrm{nm}$) set to minimum deviation to minimize the reflection losses. Since the compressor has negative group velocity-dispersion (GVD) it introduces negative chirp proportional to the prism separation. Therefore the chirp of the seed pulse could be continuously tuned from its initial positive to large negative values with different settings of the compressor length. The properly chirped pulses were fed into a 3-pass off-axis KrF amplifier [6]. The second channel of a LambdaPhysik EMG 160MSC twin-tube excimer laser served as an amplifier whose first channel was used for pumping the dye laser system. The amplifier tube was modified for off-axis operation and was equipped with 0.8-cm-thick

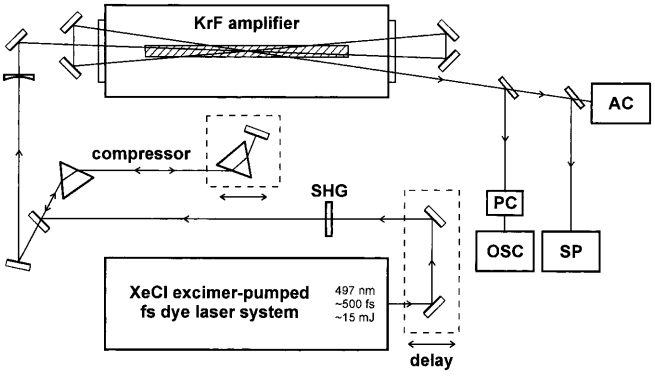

Fig. 1. Experimental layout (SHG: second-harmonic generation, PC: fast photocell, OSC: 1 GHz oscilloscope, SP: spectrograph, AC: autocorrelator)

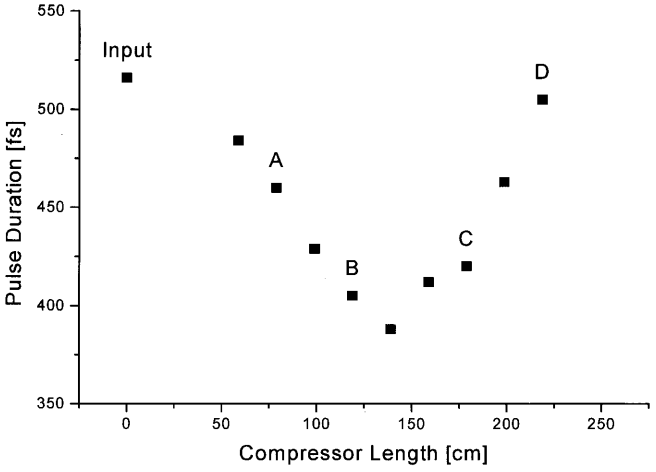

Fig. 2. Pulse durations measured after the UV amplifier as a function of the compressor length. The calculated chirp of the input pulse $\frac{\partial^2 \phi}{\partial \omega^2}$ is equal to $-23\,802$, -7934, $15\,868$ and $31\,736\,\mathrm{fs}^2$ at the A, B, C and D positions respectively

CaF_2 windows. The length and the width of the discharge were 45 cm and 0.6 cm, respectively [6] while the separation of the windows was approximately 78.5 cm. The module was filled with a standard KrF gas mixture (6 mbar F_2, 150 mbar Kr in He buffer to a total pressure of 2.4 bar). The off-axis angles were 1.3, 2.0, 2.6 degrees, respectively for the subsequent passes. The divergence of the beam was chosen to fill the full aperture of the amplifier at the end of the third pass. The energy of the input pulse was approximately 7 μJ. Proper timing of the short pulse with respect to the gain at different compressor lengths was adjusted by a variable delay line just before the frequency-converter crystal and monitored by a fast photodiode after the amplifier. The duration of the amplified pulses was measured by a multiple-shot UV autocorrelator [7] at different settings of the compressor. The results are shown in Fig. 2. which are derived by assuming Gaussian pulse shape for the deconvolution of the autocorrelation traces. The minimum pulse duration was reached at $l_0 = 139$ cm compressor length. The output spectra were recorded by a breadboard spectrograph of 1 m focal length using a 3600 g/mm holographic grating in a first-order Littrow configuration resulting in 0.2484 nm/mm linear dispersion and 0.025 nm spectral resolution.

Output spectra were recorded for different compressor settings – resulting in differently chirped input pulses – as shown in Fig. 3. In all cases the UV input spectrum was tuned to the peak of the amplified spontaneous emission (ASE) which is regarded as the center of the gain profile of the amplifying medium. A significant change in the shape of the output spectrum can be observed depending on the initial chirp introduced by the compressor while having the operational conditions of the amplifier unchanged.

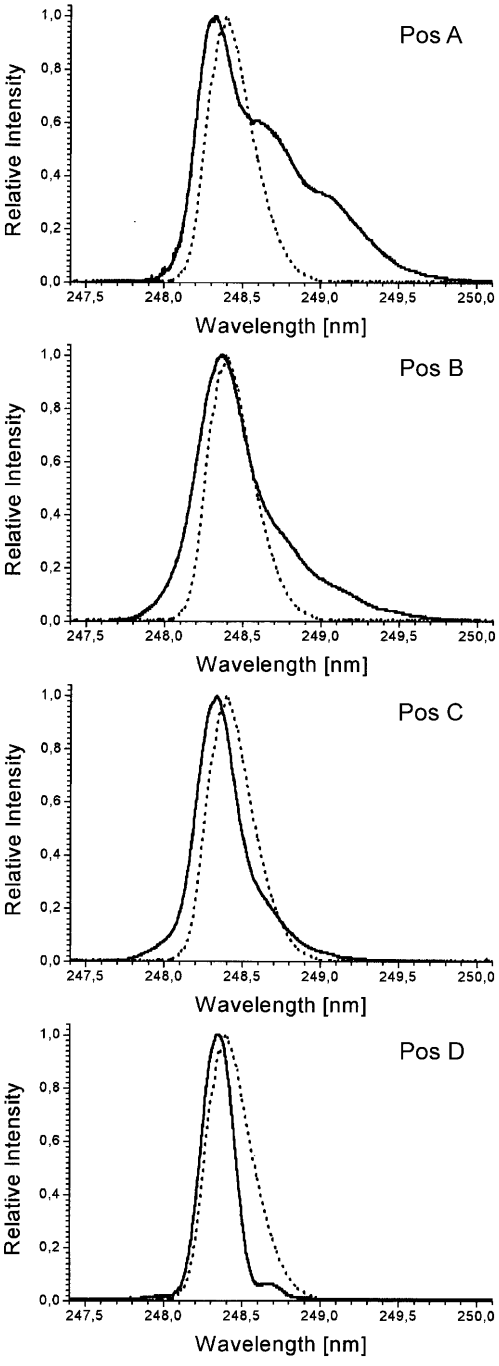

Fig. 3. Measured output spectra recorded at the signed positions of the compressor corresponding to Fig. 2. (The *dotted line* is the input, the *solid line* is the output spectrum)

2 Theory

There are different mechanisms assumed to have influence on the pulse propagation through a KrF amplifier. The most important are:

- Gain saturation changes the pulse shape by boosting up the leading edge with respect to the later parts of the pulse;
- The non-uniform gain profile of KrF [8] leads to spectral narrowing and modulation;
- The intensity-dependent refractive index of the amplifier window material results in Kerr-type self-phase modulation (SPM);
- The GVD can broaden the temporal pulse profile;
- The refractive index of the gain medium in excited and ground states is slightly different (because the material is also different, KrF^* and $Kr + F_2$ respectively), leading to

a phase change which is proportional to the fluence of the pulse and therefore causes a cumulative SPM of the pulse.

In order to see how the last effect causes SPM let us consider the overall refractive index of the gain material. Since the amplifying medium is a highly excited dense plasma generated by electronic discharge, the refractive index has contributions from ground as well as excited states, free electrons and ions in different ionization states. The index change during the light pulse which leads to SPM depends only on the population change of the ground and excited state. Therefore the overall refractive index of the gain material can be expressed by

$$n(t) = n^* + n_1\frac{N_1(t)}{N_0} + n_2\frac{N_2(t)}{N_0} = n^* + n_1 + (n_2 - n_1)\frac{N_2(t)}{N_0}\,, \tag{1}$$

where N_1 and N_2 are the numbers of molecules in the ground and excited states, $N_0 = N_1 + N_2$ is the total number of molecules and n^* is the index contribution which is not influenced by the light pulse. The refractive indices of N_0 molecules in the ground and excited states are denoted by n_1 and n_2, respectively. If all molecules are excited before the pulse enters the amplifier, the ratio of $N_2(t)$ and N_0 is equal to the ratio of the effective gain coefficient $g(t)$ and the small-signal gain coefficient g_0. Thus the phase change of the pulse travelling through the medium of length l is

$$\varphi(t) = \frac{2\pi}{\lambda_0} l\left[n^* + n_1 + (n_2 - n_1)\frac{g(t)}{g_0}\right] = \varphi_0 + \Delta\varphi(t)\,. \tag{2}$$

Here φ_0 represents the constant phase shift of the medium in the ground state. In the case of rate equation approximation (REA) and much shorter pulse durations than the relaxation time of the excited molecules (see for example [9]) the second term can be expressed by

$$\Delta\varphi(t) = \frac{2\pi}{\lambda_0} l\Delta n \exp\left[-\frac{1}{E_{\mathrm{sat}}}\int_{-\infty}^{t} I(t')\,\mathrm{d}t'\right]\,, \tag{3}$$

where $\Delta n = n_2 - n_1$, λ_0 is the central wavelength of the pulse in vacuum, E_{sat} is the saturation energy density of the gain, and $I(t)$ is the light intensity. Note that the expression for the phase variation due to carrier-induced index change in semiconductor lasers [10] has the same form as (3) with the assumption of infinitely large spontaneous carrier lifetime and the notation of

$$\alpha = 2 \times \frac{2\pi}{\lambda_0}\frac{\Delta n}{g_0}\,, \tag{4}$$

where α is the linewidth enhancement factor (see also (3) in [11]).

It is well known that the real and imaginary parts of the complex refractive index – thus the refractive index and the gain or absorption coefficient – are connected by the Kramers–Kronig (KK) relations. With the use of KK relations the refractive indices of pure excited and ground-state materials are written by

$$\begin{aligned} n_2(\omega) - 1 &= \frac{1}{\pi} P \int_{-\infty}^{\infty} \frac{-g_0(\omega')c}{2\omega'}\frac{1}{\omega - \omega'}\mathrm{d}\omega' \\ &= -N_0\frac{c}{2\pi} P \int_{-\infty}^{\infty} \frac{\sigma_{\mathrm{e}}^*(\omega')}{\omega'(\omega - \omega')}\mathrm{d}\omega'\,, \end{aligned} \tag{5}$$

$$\begin{aligned} n_1(\omega) - 1 &= \frac{1}{\pi} P \int_{-\infty}^{\infty} \frac{\alpha(\omega')c}{2\omega'}\frac{1}{\omega - \omega'}\mathrm{d}\omega' \\ &= N_0\frac{c}{2\pi} P \int_{-\infty}^{\infty} \frac{\sigma_{\mathrm{a}}(\omega')}{\omega'(\omega - \omega')}\mathrm{d}\omega' \approx \text{const.}\,, \end{aligned} \tag{6}$$

where $\sigma_{\mathrm{e}}^*(\omega)$ is the emission cross section of excited material (KrF^*), $\alpha(\omega)$ and $\sigma_{\mathrm{a}}(\omega)$ are the absorption coefficient and the absorption cross section of ground-state material ($Kr + F_2$), c is the speed of light in vacuum and P stands for the principal value integral. Since the non-excited material does not have resonance near the amplification wavelength, n_1 is approximately constant. From (5) and (6) one gets the following expression for the refractive index difference:

$$\begin{aligned} \Delta n(\omega) &= -N_0\frac{c}{2\pi} P \int_{-\infty}^{\infty} \frac{\sigma_{\mathrm{e}}^*(\omega') + \sigma_{\mathrm{a}}(\omega')}{\omega'(\omega - \omega')}\mathrm{d}\omega' \\ &\approx -\left[N_0\frac{c}{2\pi} P \int_{-\infty}^{\infty} \frac{\sigma_{\mathrm{e}}^*(\omega')}{\omega'(\omega - \omega')}\mathrm{d}\omega' + n_1\right]\,. \end{aligned} \tag{7}$$

There is a close connection between (7) and the expression of the refractive index change due to saturation in dye amplifiers [12, 13]. In our notation (2) of [12] has the form of

$$\Delta n(\omega) = -N_0\frac{c}{2\pi} P \int_{-\infty}^{\infty} \frac{\sigma_{\mathrm{e}}(\omega') + \sigma_{\mathrm{a}}(\omega')}{\omega'(\omega - \omega')}\mathrm{d}\omega'\,, \tag{8}$$

where $\sigma_{\mathrm{e}}(\omega)$ and $\sigma_{\mathrm{a}}(\omega)$ are the emission and absorption cross sections of the dye molecule. The only difference between (7) and (8) is that in laser dyes (8) the emission and absorption term in the refractive index change comes from the same molecule whereas in excimers (7) the two terms belong to different molecules yielding nonzero values of Δn far from resonance.

The short-pulse KrF amplifier is modeled by the propagation equation (similar to the one used in [9]) which accounts for most of the above-listed effects, although the dispersion of the gain profile and of Δn are neglected. Using the slowly varying envelope approximation (SVEA), rate equation approximation (REA) and local coordinates with plane wave solution the propagation equation can be written

as

$$\frac{\partial A(t,z)}{\partial z} - \frac{\mathrm{i}}{2}\left(\frac{\partial^2 k}{\partial \omega^2}\right)_{\omega_0} \frac{\partial^2 A(t,z)}{\partial t^2} = -\mathrm{i}\frac{2\pi}{\lambda_0}\frac{n_2}{2}\left|A(t,z)\right|^2 A(t,z) + \left(\frac{g_0}{2} - \mathrm{i}\frac{2\pi}{\lambda_0}\Delta n\right) \times \exp\left[-\frac{1}{E_{\mathrm{sat}}}\frac{c\varepsilon}{2n}\int_{-\infty}^{t}\left|A(t',z)\right|^2 \mathrm{d}t'\right] A(t,z)\,, \qquad (9)$$

where n is the linear refractive index, ε is the permittivity and n_2 is the nonlinear refractive index of the medium. $A(t,z)$ is the complex envelope of the electric field:

$$E(t,z) = \frac{1}{2}A(t,z)\exp\left[\mathrm{i}(\omega t - kz)\right] + \mathrm{cc}\,. \qquad (10)$$

The second term of the left side of (9) accounts for the material GVD, the first term of the right-hand side describes the effect of the Kerr-type nonlinearity and the last term on the right corresponds to the saturated amplification with the cumulative self-phase modulation. Since in our case the pulse durations are well above 100 fs, the time period of the oscillation at the central wavelength is 0.83 fs whereas the time period of the Rabi oscillation is in the order of 100 fs [14], therefore the use of SVEA and REA is realistic.

3 Calculations

Equation (9) was solved numerically by a symmetrized split-step algorithm [15, 16] for a 3-pass off-axis KrF amplifier accounting for the successive amplification passes and for the propagation in the amplifier windows before and after each pass.

Proper choice of the electric field envelope $A(t,z)$ of the input pulse is very important for the calculations. The construction of the input electric field envelope was done in the spectral domain as follows: an asymmetric Gaussian profile of the form of

$$I(\lambda) = \begin{cases} I_0 \exp\left[-4\ln 2\left(\frac{\lambda-\lambda_0}{\Delta\lambda_1}\right)^2\right] & \text{if } \lambda < \lambda_0 \\ I_0 \exp\left[-4\ln 2\left(\frac{\lambda-\lambda_0}{\Delta\lambda_2}\right)^2\right] & \text{if } \lambda > \lambda_0 \end{cases} \qquad (11)$$

was fitted to the measured input spectrum ($\lambda_0 = 248.37$ nm, $\Delta\lambda_1 = 0.23$ nm, $\Delta\lambda_2 = 0.45$ nm) and the square root of $I(\lambda)$ served for the amplitude of the spectral envelope $|A(\omega)|$.

The chirp of the input pulse before the compressor due to the saturated amplifiers and absorbers of the dye laser system is assumed to be purely linear. This does not hold thoroughly but it is still a reasonable approximation of the actual chirp. Furthermore it was also assumed that the initial chirp was completely compensated by the compressor in the case of minimum measured pulse duration. Therefore the spectral phase $\Phi(\omega)$ of the input pulse is exclusively determined by the compressor settings: it is constant zero in the compressed position and can be calculated by the

$$\Phi(\omega) = \frac{1}{2}\frac{\partial^2 \Phi}{\partial \omega^2}(\omega-\omega_0)^2 = -\frac{1}{2}\left(\frac{\partial^2 k}{\partial \omega^2}\right)_{\mathrm{comp}}(l-l_0)(\omega-\omega_0)^2 \qquad (12)$$

equation in the other positions, where $\left(\frac{\partial^2 k}{\partial \omega^2}\right)_{\mathrm{comp}} = -39.67\,\mathrm{fs}^2/\mathrm{mm}$, l is the compressor length and l_0 is the compressor length of optimal compression. The calculated chirp parameters are indicated in the caption of Fig. 2. Therefore the complex spectral envelope $A(\omega) = |A(\omega)|\exp[\mathrm{i}\Phi(\omega)]$ of the input pulse and $A(t,z)$ after the inverse Fourier transformation is fully determined.

In the calculations GVD and SPM caused by the Kerr-type nonlinearity of the amplifying medium can be neglected and only the saturated gain and the cumulative phase effects were considered. This is a good approximation because the noble-gas gain material has low dispersion and nonlinearities. For the propagation in the amplifier windows both SPM and GVD of the material (CaF_2) were considered. The physical parameters used in the calculations are listed in Table 1. For the determination of the energy densities the beam diameters were measured before and after the subsequent passes and the beam diameters were interpolated at the other planes. The output energies given by the simulation were used for the calculation of the input energy density of the next medium. Since both the beam diameter and the input energy were small (less than 1 mm and $\approx 7\,\mu$J) before the amplifier, the measured values were not accurate enough to give precise data for the input energy density of the first pass. For these reasons the input energy density was varied within a factor of 2 to give realistic energy values at the end of the amplification chain. The thickness of the amplifier windows was chosen 50% larger in the calculation than in the experiments in order to get the experimentally observed spectral broadening. The reason for the considerable difference can be explained by the inhomogeneity of the beam profile. Since most of the energy delivered by the laser beam is concentrated in hot spots, the effective area of the nonlinear interaction decreases considerably leading to higher effective intensity. This was taken into account by considering a longer interaction length. The refractive index difference between the excited and non-excited active medium was used as a fitting parameter.

Table 1. Physical parameters

Gain medium		
small-signal gain coefficient (g_0)	$0.19\,\mathrm{cm}^{-1}$	[6]
non-saturated absorption coefficient (α)	$0.019\,\mathrm{cm}^{-1}$	[6]
saturation energy density (E_{sat})	$2.1\,\mathrm{mJ/cm}^2$	[6]
refractive index difference (Δn)	1.98×10^{-7}*	
effective length in 1st pass (l_1)	26.45 cm**	
effective length in 2nd pass (l_2)	17.19 cm**	
effective length in 3rd pass (l_3)	13.23 cm**	
Window material		
nonlinear refractive index (γ)***	$1.92\times10^{-16}\,\mathrm{cm}^2/\mathrm{W}$	[17]
GVD parameter $\left(\frac{\partial^2 k}{\partial \omega^2}\right)$	$145.5\,\mathrm{fs}^2/\mathrm{mm}$****	
length (l)	1.2 cm	

* This value corresponds to $\approx 3.1\%$ of the refractive index of 12 mbar Kr + 6 mbar F_2 gas mixture [18].
** Calculated from the discharge dimensions and the applied off-axis angles.
*** $n_2 = \frac{c\varepsilon}{n}\gamma$, $n_{\mathrm{total}} = n + n_2\langle E^2(t)\rangle_{\mathrm{T}} = n + \gamma I(t)$
**** Calculated from the dispersion formula given in [19]

4 Discussion

The calculated spectra and pulse shapes for different initial chirp parameters are shown in Figs. 4 and 5 and the most important calculated parameters are listed in Table 2. The calculated spectral profiles are in good agreement with the experimentally recorded ones (Fig. 3.). The similarity is remarkably good if we consider that the complex envelope function of the input pulse was not known exactly and the spectral effects of the finite gain bandwidth were not taken into account. The main feature of the output spectra seen on both Figs. 3. and 4. is the significant asymmetric spectral broadening in the case of positively chirped input pulse and the

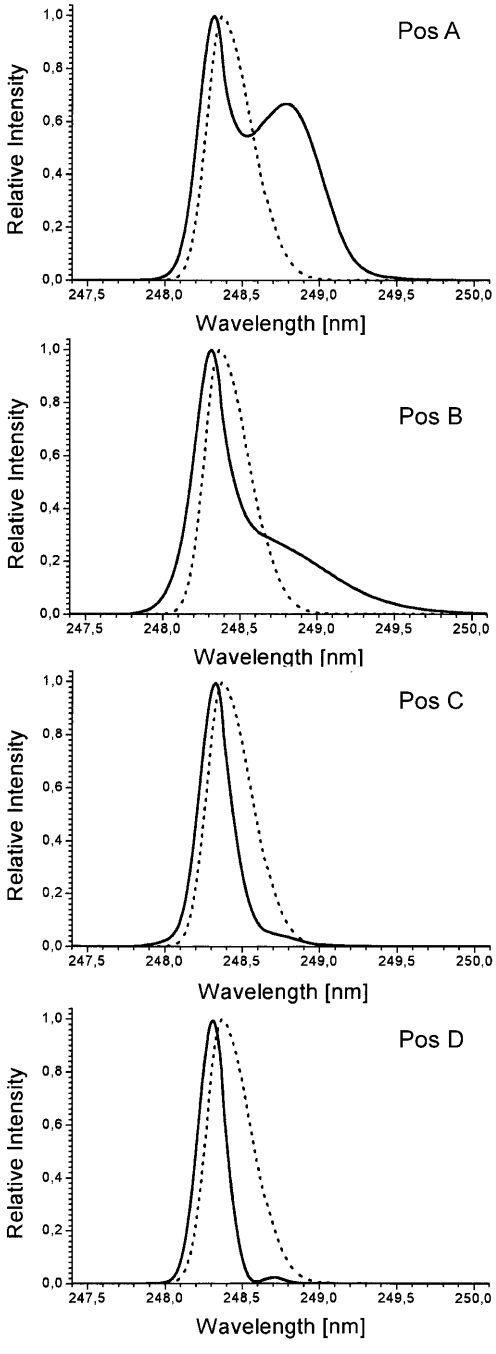

Fig. 4. Calculated output spectra (The notations are the same as in Fig. 3)

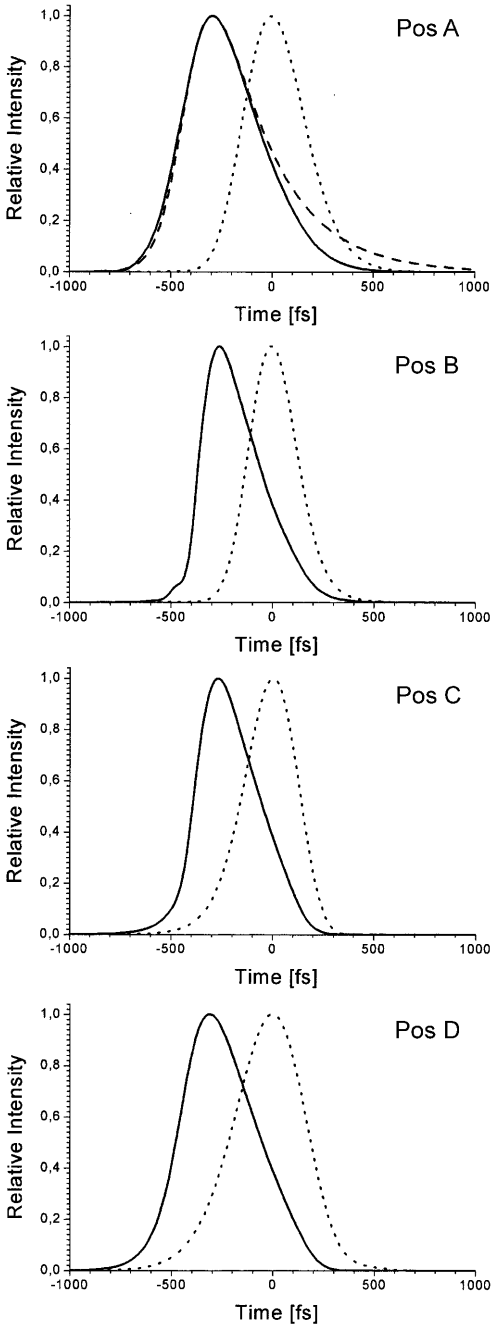

Fig. 5. Calculated pulse shapes (The *dotted line* is the input, the *solid line* is the output pulse shape. Asymmetric sech^2 pulse shape determined by Le Blanc et al. [20] is indicated by dashed line at position A)

spectral narrowing when the input had negative initial chirp. The calculations with different sets of parameters show that the Kerr-type SPM in the window material has the major influence on the spectral properties of the output pulse. This is demonstrated in Fig. 6, where only the SPM of the laser windows was taken into account resulting in the same overall nonlinear phase shift (the so-called B-integral, see Table 2) as in the calculation using (9).

There are two possible interpretations of the observed asymmetric spectral broadening effect. According to the first one the time-dependent frequency-shift due to SPM adds to a positive initial chirp resulting in much more pronounced

Table 2. Calculated parameters ($E_{out} = 11.94$ mJ in all cases)

	Pulse duration (FWHM) input	output	Overall B-integral*
Pos A	352 fs	432 fs	1.61
Pos B	275 fs	320 fs	2.11
Pos C	305 fs	342 fs	1.86
Pos D	406 fs	426 fs	1.47

* $B = \max \frac{2\pi}{\lambda_0} \int_0^l \gamma I(t, z) \mathrm{d}z$

broadening than for a transform-limited pulse. On the other hand the frequency modulation introduced by SPM can cancel a negative initial chirp which leads to spectral narrowing [21]. The other possible explanation is that the SPM of an asymmetric pulse leads to the observed asymmetric spectral broadening: the broadening on the long wavelength side which is governed by the steeper leading edge is larger than the broadening on the blue side influenced by the falling edge of the pulse [22]. The narrowing effect observed at positions C and D, however, cannot be interpreted this way since SPM alone always leads to spectral broadening. Only the interplay of the initial chirp and the counteracting SPM can explain the experimentally observed dependence of the broadening on the initial chirp.

The SPM due to the different refractive index of the excited and non-excited gain material results in a spectral shift and an asymmetric broadening towards shorter wavelengths. (Its effect can be seen for example in Fig. 3 of [10]. In our case $\alpha_{\text{equivalent}} = 0.53$.) In KrF amplifiers this effect is less pronounced than the Kerr-type SPM, however the spectral shape of the output pulses are determined by the linear combination of the SPMs from different origins. The GVD in the window material plays a passive role in the spectral evolution of the pulse since its only influence is to decrease the energy density via pulse broadening resulting in a lower level of SPM.

Although the present paper concentrates on the spectral properties of the amplification process, it is also interesting to see the calculated temporal pulse shapes which are displayed in Fig. 5. There the input and output temporal profiles are denoted by dotted and solid lines, respectively. Although the shape of the input pulses varies considerably with the compressor length (it is asymmetric with steeper leading edge at position A, almost symmetric at B and asymmetric with steeper falling edge at C and D), the shape of the output pulses is always asymmetric with sharp leading and gently sloping trailing edges mainly due to the saturation of the gain. The calculated output pulse durations (Table 2) are all shorter by a factor of ≈ 1.2 than the ones derived from the autocorrelation measurements which also indicates that the symmetrical Gaussian pulse profile is not the most adequate choice for the deconvolution of the autocorrelation traces. It is interesting to compare these pulse shapes to that determined by Le Blanc et al. [20] from numerical fitting of a single-shot phase-sensitive autocorrelation trace of the output pulse (indicated at position A of Fig. 5 by dashed line). Our calculations show a pulse shape with similar leading edge but less pronounced tail at position A in which the input parameters were close to those used in [20]. The output pulses have considerable amount of positive chirp due to the material GVD and the chirping effect of the SPM. The minimum pulse durations that can be achieved by a quadratic pulse compressor after the amplifier are also calculated yielding 156 fs, 115 fs, 213 fs and 312 fs which means 2.77, 2.78, 1.61 and 1.36 compression ratio at positions A, B, C and D, respectively. Note that further increase of the bandwidth and decrease of the minimum pulse duration can be achieved by tuning the input pulse to the shorter wavelength side of the gain profile. The minimum pulse duration routinely achieved by compression after amplification is below 100 fs measured by autocorrelation technique with the assumption of

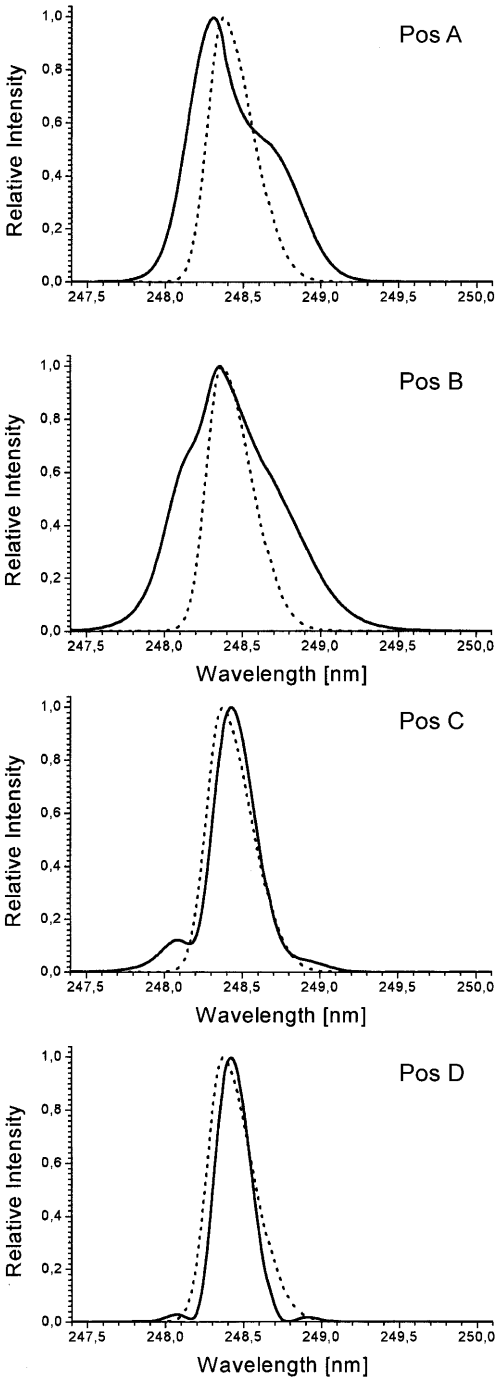

Fig. 6. Output spectra calculated with only Kerr-type SPM in windows taken into account. (The notations are the same as in Fig. 3)

a Gaussian profile. In conclusion it is found that the spectral broadening due to SPM can greatly be influenced by proper choice of the input chirp parameter. A moderate positive chirp leads to spectral broadening whereas a negative input chirp decreases the bandwidth. This effect has major importance in optimizing short-pulse KrF amplifiers for the maximum achievable bandwidth for minimum final pulse duration.

Acknowledgements. The authors wish to thank M. Feuerhake for valuable discussions. This work has been supported by the K+F program of the Hungarian Ministry of Education (contract FKFP 1103/1997), by the Hungarian OTKA Foundation (contract T 029179), by the TÉT British–Hungarian Cooperation (contract GB-29/96) and the NATO Science for Peace Programme (SfP-971989).

References

1. S. Watanabe, A. Endoh, M. Watanabe, N. Sarukura, K. Hata: J. Opt. Soc. Am. B **6**, 1870 (1989)
2. I.N. Ross, A.R. Damerell, E.J. Divall, J. Evans, G.J. Hirst, C.J. Hooker, J.R. Houliston, M.H. Key, J.M.D. Lister, K. Osvay, M.J. Shaw: Opt. Commun. **109**, 288 (1994)
3. S. Szatmári, G. Almási, M. Feuerhake, P. Simon: Appl. Phys. B **63**, 463 (1996)
4. S. Szatmári: Appl. Phys. B **58**, 211 (1994)
5. J.R. Houliston, I.R. Ross, M.H. Key, S. Szatmári, P. Simon: Opt. Commun. **104**, 350 (1994)
6. G. Almási, S. Szatmári, P. Simon: Opt. Commun. **88**, 231 (1992)
7. S. Szatmári, F.P. Schäfer: Opt. Commun. **68**, 196 (1988)
8. M.J. Shaw, E.J. Divall, G.J. Hirst, C.J. Hooker, J.M.D. Lister, I.N. Ross, A. Kvaran, K. Osvay: J. Chem. Phys. **105**, 1815 (1996)
9. A. Dienes, L.W. Carr, M.-Y. Hong: IEEE J. Quant. Electron. **QE-27**, 1214 (1991)
10. G.P. Agrawal, N.A. Olsson: IEEE J. Quant. Electron. **QE-25**, 2297 (1989)
11. M. Osinski, J. Buus: IEEE J. Quant. Electron. **QE-23**, 9 (1987)
12. M.A. Vasileva, A.V. Masalov, J. Vishchakas, V. Gulbinas, V. Kabelka, V. Syrus: Appl. Phys. B **37**, 41 (1985)
13. Zs. Bor, G. Szabó, F. Ráksi: *In Ultrafast Phenomena in Spectroscopy UPS'87*, ed. by Z. Rudzikas, A. Piskarskas, R. Baltramiejunas (World Scientific, Singapore 1987) p. 33
14. P.W. Milonni, R.B. Gibson, A.J. Taylor: J. Opt. Soc. Am. B **5**, 1360 (1988)
15. P. Heist, W. Rudolph, V. Petrov: Appl. Phys. B **49**, 113 (1989)
16. G.P. Agrawal: *Nonlinear Fiber Optics* (Academic Press, San Diego 1989) pp. 44–48
17. Y.P. Kim, M.H.R. Hutchinson: Appl. Phys. B **49**, 469 (1989)
18. Landolt-Börnstein: *Physikalisch-Chemische Tabellen*, 4. Auflage (Springer, Berlin 1912) pp. 1017–1019
19. A. Feldman, D. Horowitz, R.M. Walker, M.J. Dodge: NBS Technical Note 993 (1979)
20. S.P. Le Blanc, G. Szabó, R. Sauerbrey: Opt. Lett. **16**, 1508 (1991)
21. E.T.J. Nibbeling, M.A. Franco, B.S. Prade, G. Grillon, J.-P. Chambaret, A. Mysyrowicz: J. Opt. Soc. Am. B **13**, 317 (1996)
22. S.P. Le Blanc: PhD Thesis (Rice University, Houston 1994) p. 27